Evaporation-induced flow around a pendant droplet and its influence on evaporation

S. Somasundaram, T. N. C. Anand, and Shamit Bakshi

Evaporation-induced flow around a pendant droplet and its influence on evaporation

S. Somasundaram, T. N. C. Anand,[a)] and Shamit Bakshi[b)]

*Department of Mechanical Engineering, Indian Institute of Technology Madras,
Chennai 600036, India*

Studies on the evaporation of suspended microlitre droplets under atmospheric conditions have observed faster evaporation rates than the theoretical diffusion-driven rate, especially for rapidly evaporating droplets such as ethanol. Convective flow inside rapidly evaporating droplets has also been reported in the literature. The surrounding gas around the evaporating droplet has, however, been considered to be quiescent in many studies, the validity of which can be questioned. In the present work, we try to answer this question by direct experimental observation of the flow. The possible causes of such a flow are also explored. © *2015 AIP Publishing LLC.*
[http://dx.doi.org/10.1063/1.4935355]

I. INTRODUCTION

The process of droplet evaporation according to Maxwell's equation[1] is described on the basis of pure diffusion of the evaporating species through the surrounding medium. However, the experimental evaporation rate has been observed to be higher than the diffusion-driven evaporation rate, especially for rapidly evaporating pendant droplets.[2,3] It is now understood that the process of diffusion alone is insufficient to describe the evaporation process, even under atmospheric conditions, as many other accompanying processes can influence the evaporation rate.

One of the pertinent processes which influences the evaporation rate is internal circulation.[2,4,5] Hegseth, Rashidnia, and Chai[4] observed an internal circulation inside an evaporating methanol droplet suspended from a loop under atmospheric conditions, due to surface tension gradients. They also mentioned the possibility of flow outside the droplet resulting from shear at the interface, but they did not confirm the presence of flow in the surroundings experimentally. However, this contrasts with the inference of Guèna *et al.*,[6] which they utilized in theoretical modelling of sessile droplets of water, alkanes, etc. They used a stationary diffusion assumption to model the evaporation of hydrophilic liquids on a silicon wafer substrate. To justify their assumption, they performed experiments with suspended and sessile droplets using the same substrate and observed that the evaporation rates (exponents) were similar for both. They argued that a sessile droplet of water is more likely to have convection around it, as water vapour is lighter than air, whereas a suspended drop of an alkane is more likely to have convection around it, as alkane vapour is heavier than air. Equality of the evaporation rates for suspended and sessile droplets for each of the liquids led them to conclude that convection is not important in this situation. In a recent work by Chini and Amirfazli,[3] the applicability of the quasi-steady assumption as well as that of the pure-diffusion assumption in the Maxwellian model of droplet evaporation was examined for a suspended pendant droplet under atmospheric conditions. They showed that relaxing the quasi-steady and pure-diffusion assumptions could lead to quite different results, particularly for rapidly evaporating droplets. They point towards the presence of convection around the droplet, even under atmospheric conditions.

Indications of the presence of convection around sessile droplets had come previously from the use of an interferometric technique to identify vapour clouds.[7] However, more definite interferometric

---

a)Electronic mail: anand@iitm.ac.in
b)Electronic mail: shamit@iitm.ac.in

evidence of vapour clouds around pendant droplets indicating the presence of convection was reported recently by Dehaeck, Rednikov, and Colinet.[8] They suspended a droplet of 3M Novec HFE-7000 (engineered fluid) from a silicon wafer and made measurements under atmospheric conditions. This fluid is highly volatile and its vapour is considerably heavier than air, resulting in a large value of the Grashof number (≈ 852, considering the solutal contribution alone). The Grashof number is defined as the ratio of the buoyancy force to the viscous force. The high values of the density gradient and surface concentration were warranted by the interferometric technique used. These measurements and simulations show that inclusion of the effects of convection around a suspended droplet along with Marangoni convection in the interface is critical for correct prediction of local and global evaporation rates. The local evaporation rates are also important in the context of hydrothermal instabilities[9,10] which are more pronounced during the intermediate stages of evaporation[11] and are thermocapillary in origin.[12]

Experimental evidence of flow around a sessile droplet under ambient conditions was reported by Kelly-Zion *et al.*[13] using schlieren imaging. Using microgravity experiments, Carle, Sobac, and Brutin[14] confirmed the presence of flow around a sessile droplet by comparing the evaporation rate with the diffusion-driven rate. Dunn *et al.*[15] included ad hoc corrections to the diffusion model to incorporate the buoyancy effect of water vapour for an evaporating sessile droplet. With this correction, they were able to obtain a good comparison with experimental results. This indicates that convection could be present for this situation. Saada, Chikh, and Tadrist[16] also considered buoyancy-driven convection in their numerical simulation and justified the inclusion of the buoyancy correction in the earlier work of Dunn *et al.*[15] As already mentioned, the recent work by Dehaeck, Rednikov, and Colinet[8] measured vapour concentration around a pendant droplet using an interferometric technique that clearly shows convective flow for a Grashof number of 852. For such a high Grashof number, convective flow is quite likely. It is not easy, however, to extend these observations to deduce the presence of convective flow in a pendant droplet for low Grashof numbers. The above-mentioned studies also did not provide direct evidence in terms of flow velocity measurement. This is significant particularly because the existence of flow can be independent of its influence on the evaporation rate. In other words, the flow may exist but need not significantly influence the evaporation rate. For example, although it is apparent from the work of Kelly-Zion *et al.*[13] and Carle, Sobac, and Brutin[14] that evaporation-induced convection exists around an evaporating sessile droplet, the work reported by Gelderblom *et al.*[17] shows that the model of Popov,[18] which is based on the pure-diffusion assumption, accurately describes the evaporation rate. Similarly, Sefiane *et al.*[19] modified the basic diffusion-based model to take into account the effect of the change in diffusivity due to temperature and the surrounding gas, as well as the thermal conductivity of the substrate, and found a good match with experimental measurements. The recent work of Gleason and Putnam[20] also indicates that a modified diffusion-controlled model with corrections for the non-uniform surface vapour concentration can predict accurately the evaporation rate of a sessile droplet of water. These results suggest that free convection does not contribute to evaporation under the conditions used in these studies, although they do not rule out its presence. Hence, in the present paper, we rely on direct evidence for the existence of flow using velocimetry for evaporating pendant droplets (but not for sessile droplets). Thus, the first question addressed in this paper is as follows: Does a flow exist around a pendant droplet evaporating under ambient conditions for low Grashof numbers? Second, if there is a flow, what causes this flow?

We explore different methods to address these questions, and we believe that the experimental results presented in this paper give conclusive answers to them.

II. EXPERIMENTAL SETUP AND METHOD

A schematic of the setup used in the present experimental study is shown in Fig. 1. The setup included the test rig, systems to create the droplet and a controlled environment, and diagnostic equipment, all of which were mounted on an optical breadboard. The test rig was a cubical chamber of length 24 cm with a metal frame. Five sides of the chamber had glass plates fixed to the frame with silicone rubber gaskets to ensure a leakproof fitting, while the top was made of clear acrylic.
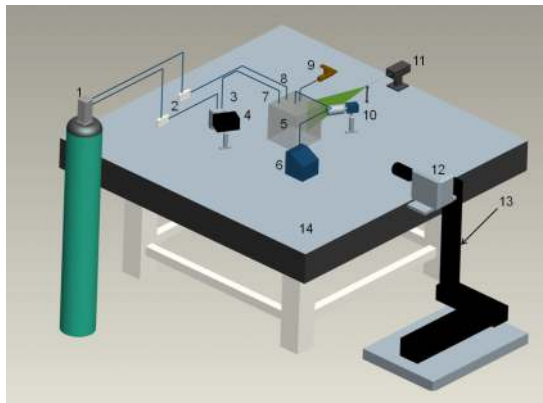
FIG. 1. Schematic of experimental setup: 1, cylinder for gas supply; 2, solenoid valves; 3, seeding-particle generator; 4, strobe light; 5, test rig; 6, syringe pump; 7, inlet for seeding particles; 8, inlet for gas; 9, outlet; 10, CCD camera; 11, laser; 12, CMOS camera; 13, micro-control traverse; and 14, optical table.

The top plate of the chamber also had provision through solenoid-controlled valves to introduce fresh gas, to introduce seeding particles, and to purge the ambient gas from the chamber. The seeding particles used were small sesame oil droplets produced using a generator fabricated following the design of Jermy.[21] The measured particle size distribution of these particles (measured using a phase Doppler interferometer) indicated that their mean size was around 2 μm. The chamber was also fitted with a K-type thermocouple to measure the ambient temperature.

A stainless steel needle of inner diameter 2.6 mm, length 140 mm, and thickness 0.5 mm, with a flat tip, was inserted from the centre of the top plate. A droplet of known volume (with an initial equivalent diameter of 3.1 ± 0.1 mm) was repeatably suspended at the lower end of this needle by operating a syringe pump fitted with a 25 ml Hamilton syringe, which was connected to the needle. A light-emitting diode (LED) strobe backlight and a 14-bit charge-coupled device (CCD) camera of resolution 1392 × 1040 pixels, with a 105 mm macrolens, were triggered using a National Instruments TTL module to acquire images of the droplet at 10 s intervals. A green (532 nm) beam of diameter 1.1 mm from a continuous diode-pumped solid-state (DPSS) laser was expanded using a 20 mm focal length plano-convex cylindrical lens to form a vertical laser sheet. This was passed through the chamber to illuminate a region of height 85 mm. To avoid reflections from the droplet, the top of the laser sheet was positioned about 6–10 mm below the droplet. A high-speed complementary metal-oxide semiconductor (CMOS) camera (with a resolution of 1024 × 1024 pixels) fitted with a 50 mm lens was used to take images of the seeding particles. In some of the experiments, for measurement of droplet surface temperature, thermal images of the droplet were taken through a provision in one of the side plates of the chamber using a thermal imaging camera (with a resolution of 320 × 240 pixels).

The experimental procedure was standardized as follows. The test chamber was first purged with nitrogen (99% pure) from a nitrogen cylinder at a pressure of 2 bar for 60 s by opening a solenoid valve. The chamber was then filled with seeding particles by opening the appropriate solenoid valves for 1 s. Then, to reduce the seeding density, nitrogen gas from the cylinder was again introduced into the chamber for 10 s with the outlet line open. Both valves were then closed, and any flow still present in the chamber was allowed to subside for 120 s. A droplet of the test fluid (99.9% pure ethanol or HPLC-grade water) was then created by operating the syringe pump at a low flow rate (250 μl/min), to discharge a fixed volume. Backlit images of the droplet were acquired using the CCD camera and LED backlight. These images were processed with a code written in Matlab to determine the evaporation rate as a function of time. Images of the seeding particles were acquired using the laser sheet and the high-speed camera. The procedure was repeated eight times for each condition. The particle image velocimetry (PIV) images were processed with the open-source "PIV-LAB" software[22,23] to obtain the velocities. The images were well correlated, with a correlation coefficient greater than 0.75. For some experiments, the metallic needle was

replaced by a quartz fibre with a bead of diameter 1.3 mm at the tip, from which a droplet of 2.1 ± 0.1 mm size was suspended. Streak images of the particles surrounding the droplet were also obtained using a laser sheet and a camera set to a high exposure time (50 ms).

III. RESULTS AND DISCUSSION

A. Is there a flow around the evaporating droplet?

To determine whether flow existed around the droplet, the chamber was seeded using small oil particles using the method described above. Streak images were obtained, an example of which for an evaporating ethanol droplet is shown in Fig. 2. The streaking in the illuminated region just below the droplet clearly indicates the presence of flow below the droplet evaporating at atmospheric temperature and pressure. The videos available online indicate the same: Movie 1[24] shows the flow below a pendant ethanol droplet, while Movie 2[24] shows the flow below an evaporating water droplet. Images were taken at 50 frames/s in both cases and are played back at 5 frames/s.

The flow below the droplet is in the form of a downward plume. This flow was observed even for slowly evaporating water droplets and both for droplets suspended from the metallic needle and for those suspended from the quartz fibre. Fig. 3 shows the velocity profile along a line perpendicular to the needle axis, at 50 mm below the droplet, for an evaporating water droplet (suspended from a metallic needle) and for an ethanol droplet (suspended from a metallic needle or a quartz fibre). The velocity profiles for these cases are at an instant when the diameter of a volume-equivalent sphere is 3 mm for the metallic needle case and 2 mm for the quartz suspender case. The peak velocities and the extent of the disturbed region are comparable, within the range of experimental uncertainties for these cases. As expected, the flow changed when the evaporating liquid and the ambient gas were changed; those results will be reported separately and are not the focus of the present study.

The development of the flow was studied through a long distance downwards from the tip of the needle. Fig. 4 shows the velocity profile (non-dimensionalized) at a given time for 47 different stations from the tip of the needle, varying from an axial distance of around 5–25 times the needle-diameter. The time corresponding to this plot is 100 s (droplet diameter = 2.46 mm) after the start of the evaporation process. The velocity is non-dimensionalized with the maximum velocity at a given station and the distance with the radial distance at which the velocity reaches half the maximum velocity. Certain interesting features are apparent from this figure. The collapsing of the velocity profile is an indication of its self-similar characteristics as observed in buoyant plumes. The extent of the disturbed region is seen to be around 4–5 times the radial distance at which half
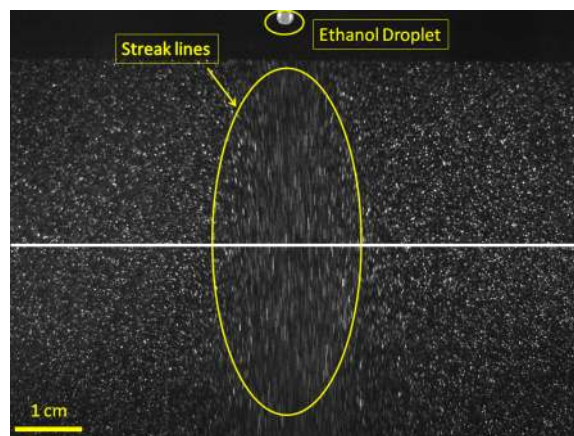

FIG. 2. Streaking image showing the flow below an evaporating ethanol droplet. The white horizontal line indicates the location of the velocity profile measurements shown in Fig. 3. The contrast of the image has been enhanced to make the droplet visible.
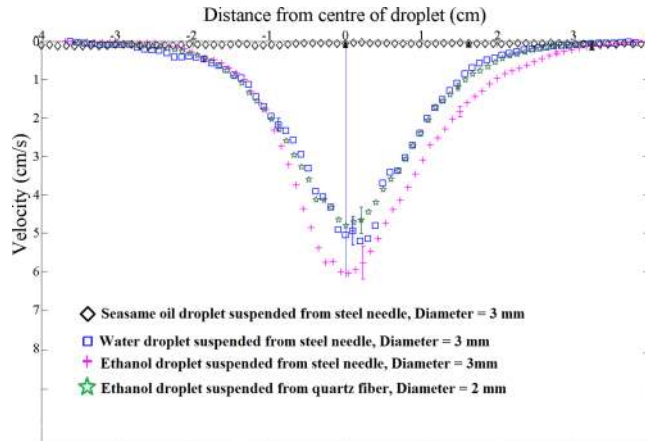
FIG. 3. Velocity (vertical component) variation with distance from the suspender axis for an evaporating water droplet and the evaporating ethanol droplets. The velocity is measured 50 mm below the tip of the suspender. The central vertical line is the axis of the suspender. Positive values indicate downward flow. The diameter indicated is the volume-equivalent diameter of the droplet.

the maximum velocity is reached. This is roughly 10 times the needle diameter on each side of the axis. This is different for the case of the water droplet where the disturbed region is around 12–13 times the needle diameter on each side of the axis.

In the work described here, we investigated whether the flow was really from the evaporating droplet or whether there could be any other possible source for the flow. With this aim, the background flow was characterized by PIV. The velocity magnitudes in the absence of the needle were very small, with a mean of 0.07 cm/s and a standard deviation of 0.015 cm/s. Experiments were also performed with the needle inserted in the chamber but without introducing the drop, and again the velocities observed were very small and of a similar order. To confirm that the flow was due to evaporation, we performed experiments with sesame oil. The sesame oil droplet did not evaporate under the present conditions and remained unchanged in diameter for hours. The droplet insertion process (with an insertion rate of about 250 μl/min) and other parameters for this experiment were maintained similar to those in the experiments done with the evaporating liquids (water and ethanol). The velocity profiles for these cases are shown in Fig. 3. The flow field and the velocity histogram (for the vertical component of velocity) are shown in Fig. 5 (note that downward

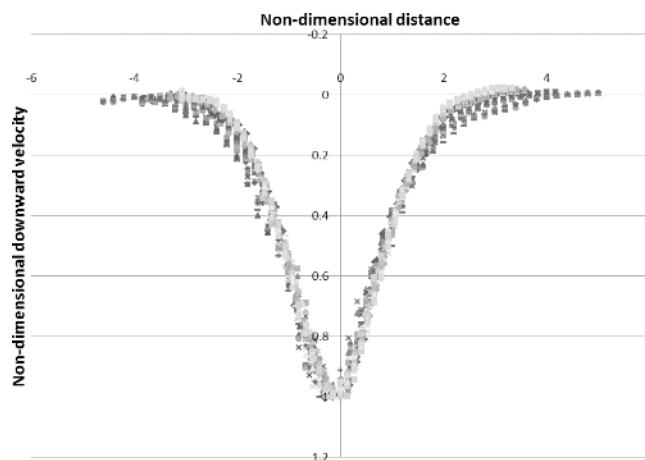FIG. 4. Non-dimensional velocity (vertical component) variation with non-dimensional distance at various locations (47 stations) below an evaporating ethanol droplet. The velocity is non-dimensionalized with the maximum velocity at a given station and the distance with the radial distance at which the velocity reaches half the maximum velocity. The profiles correspond to a time t = 100 s after the start of evaporation.
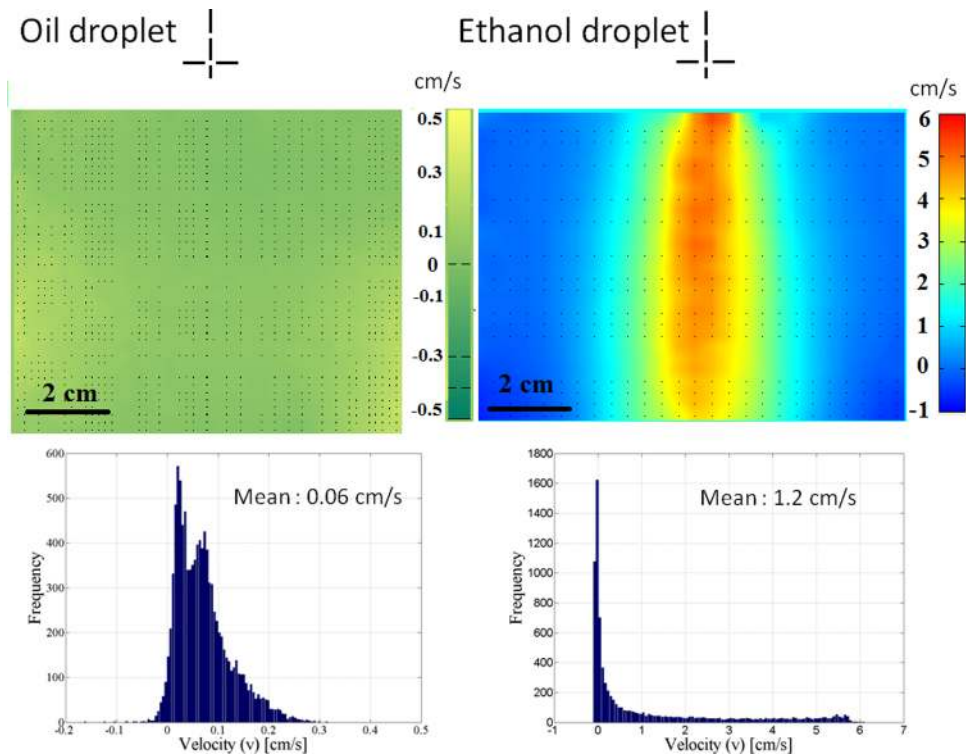
FIG. 5. Comparison of the vertical component of velocity field (top) and velocity histogram (bottom) for the non-evaporating (left) and evaporating droplets (right). The mean values indicated in the lower figures are for the entire window. The cross wires at the top indicate the tip of the needle.

movement is considered positive here). It can be seen that the flow with the suspended sesame oil droplet is of the same order as the background velocity, with a magnitude of about 0.08 cm/s. Hence, we can conclude that considerable velocities with a definite flow pattern are only observable in the case of evaporating droplets. The velocity histogram for the oil droplet shows a bias towards positive, i.e., downward velocity. This probably indicates slow settling of the small particles under gravity in the absence of evaporation-induced flow.

Flow of significant magnitude, as shown in the right hand side panel of Fig. 5, was only observed when an evaporating droplet such as water or ethanol was present, and, indeed, the flow subsided once the droplet had evaporated and disappeared. Hence, from the present experiment, we conclude that there is indeed flow around the evaporating droplet under atmospheric conditions and that it originates from the evaporation process itself. In fact, during the experiments, it was not possible to achieve a perfectly quiescent ambient medium in the presence of an evaporating droplet.

B. What causes the flow?

Having observed the flow around the droplet, it is important to identify what causes this flow. Experiments were performed to understand the mechanism of the flow. As the droplet evaporates, vapour is released into the surrounding gas. This vapour can be lighter or heavier than the surrounding medium, depending on two factors, namely, its temperature (which is essentially the temperature of the droplet surface) and its molecular weight. Under the present conditions, the temperature of the droplet surface is always less than that of the ambient gas, due to evaporative cooling. Temperature measurements with the infrared (IR) camera indicated that the temperature of an evaporating ethanol droplet suspended from a steel needle was $16.2 \pm 1\,°C$ at an ambient (nitrogen) temperature of $28 \pm 1\,°C$. The corresponding temperature for water was $19.6 \pm 1\,°C$ in the same ambient gas. The molecular weight of the vapour can be higher (ethanol in a nitrogen atmosphere)

or lower (water in nitrogen) than that of the ambient gas, depending upon the liquid–gas combination. Therefore, the observed flow could result from the net difference in density between the evaporating gas and the surrounding gas. This density difference determines the buoyancy force and is accounted for in the Grashof number, which is expressed as

$$Gr = \frac{g \Delta \rho R^3}{\nu_g^2 \rho_g}, \tag{1}$$

where g (9.81 m/s^2) is the acceleration due to gravity, R is the outer radius of the needle, ν_g is the kinematic viscosity of the ambient gas, and ρ_g is the density of the ambient gas. The pendant droplets are pinned along the contact line at the needle edge till the end of evaporation. Hence, the needle radius (rather than the droplet diameter) is used as the length scale for convection. $\Delta \rho$, which is the net density difference causing the flow, is given by

$$\Delta \rho = \rho \left[\frac{M_v - M_g}{M} (x_s - x_\infty) - \left(\frac{T_s - T_\infty}{T} \right) \right]. \tag{2}$$

Here, M is the mixture molecular weight, x_s is the mole fraction of the vapour at the droplet surface, and x_∞ is the mole fraction far away from the droplet (0 in the present case). ρ is the mixture density calculated at an average temperature of $\frac{1}{2}(T_s + T_\infty)$ and mole fraction of the vapour of $\frac{1}{2}(x_s + x_\infty)$. M_v is the molecular weight of the vapour and M_g is the molecular weight of the gas. T_s and T_∞ are the droplet surface and ambient temperatures, respectively, and T is the average of these two temperatures. Note that this definition of the Grashof number accounts for both thermal and solutal effects, either of which could dominate. With the solutal effect alone, and considering $T_s = T_\infty$, this reduces to the expression given by Dehaeck, Rednikov, and Colinet.[8] The values of the Grashof number for all the present experiments are shown in Table I. It is observed that the values of the Grashof number are very low for the present case and are less than 10. This means that the buoyancy force and the viscous force are comparable to each other. Hence, the question arises whether this is enough for buoyancy-driven convection.

The second possible mechanism generating the flow could be the momentum flux of the vapour leaving the droplet surface due to evaporation. To investigate this further, we created an equivalent situation by introducing gaseous nitrogen or carbon dioxide through the needle at a volumetric flow rate and momentum flux close to those produced by the ethanol vapour generated from droplet evaporation in the ambient nitrogen gas. This experiment was done by filling a syringe from a gas cylinder and then introducing the nitrogen or carbon dioxide from the needle using the syringe pump. The idea behind this experiment was to isolate the effects of the two possible mechanisms, namely, the momentum flux induced by evaporation and the buoyant flow due to density difference. Buoyant forces will be absent in the case of nitrogen injected into ambient nitrogen, but the momentum flux due to introduction of the gas will be present. It should be noted that carbon dioxide has a similar molecular weight (44 kg/kmol) to ethanol (46 kg/kmol) and hence will provide a close representation of the effect of molecular weight on density. Thus, with a similar momentum flux as that due to evaporation, the experiment injecting nitrogen into nitrogen represents the same momentum flux condition in the absence of a density gradient, while the injection of carbon dioxide into nitrogen represents the combined effect of a momentum flux and a density

TABLE I. Data for evaporating ethanol and water droplets suspended from a metallic needle and a quartz fibre (volume-equivalent droplet diameter = 2 mm and T_∞ = 301 K).

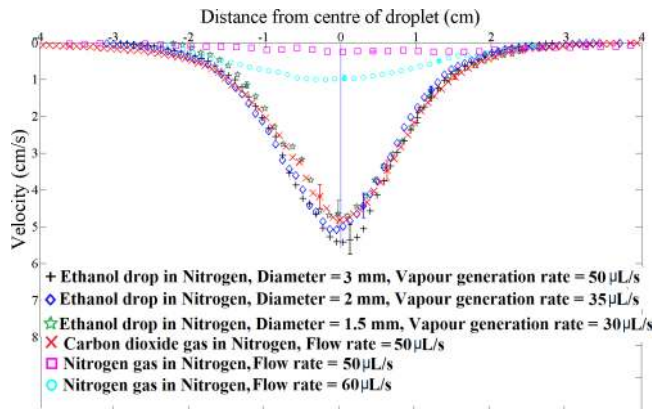| Configuration		T_s (K)	Evaporation rate (mg/min)	Evaporation rate (diffusion-driven) (mg/min)	$Gr_{Solutal}$ (no unit)	$Gr_{Thermal}$ (no unit)	Gr (no unit)
Suspender	Liquid						
Steel	Ethanol	288	5.5	0.74	2.3	3.8	6
Quartz	Ethanol	283	0.8	0.52	1.7	5.3	6.9
Steel	Water	293	0.5	0.33	−0.7	2.3	1.6
Quartz	Water	288	0.21	0.27	−0.5	3.2	2.6

FIG. 6. Velocity (vertical component) variation with distance from the needle axis for gas flow and an evaporating ethanol droplet. The velocity is measured at 50 mm below the needle tip. The central vertical line is the axis of the needle. Positive values indicate downward flow. The diameter indicated for the evaporating droplet is the volume-equivalent diameter at that particular instant during evaporation.

gradient (only solutal). The momentum flux to be imposed was calculated by obtaining the average velocity, i.e., volumetric flow rate (of evaporated vapour from the ethanol droplet) per unit needle flow area. The product of the density of the gas or vapour and the square of the average velocity is the momentum flux. Using this method, the momentum flux for nitrogen injected into nitrogen at a flow rate of 60 μl/s is 0.147 mN/m^2, that for carbon dioxide injected into nitrogen at a flow rate of 50 μl/s is 0.156 mN/m^2 and that for an ethanol droplet with a vapour generation rate of 50 μl/s is 0.163 mN/m^2. The results of this study are presented in Fig. 6, which shows the velocity profiles at 50 mm from the needle tip for an ethanol droplet evaporating in ambient nitrogen (at three different times corresponding to diameters of 3, 2, and 1.5 mm), carbon dioxide injected into ambient nitrogen at an injection rate of 50 μl/s (close to that in the evaporation case), and nitrogen injected into ambient nitrogen at injection rates of 50 and 60 μl/s.

As can be seen from Fig. 6, the flow induced by the injection of nitrogen into ambient nitrogen, at flow rates (of 50 and 60 μl/s) similar to the vapour generation rate, is very small compared to the flow induced by the evaporating droplet. The flow induced by nitrogen in ambient nitrogen at a similar momentum flux is smaller than that induced by carbon dioxide in nitrogen or by ethanol in nitrogen. Hence, the observed flow is predominantly not due to the momentum flux of vapour leaving the evaporating surface. It can also be noted from the figure that the momentum flux, although small, need not be negligible, as can be seen in the case of a nitrogen flow rate of 60 μl/s.

Injection of carbon dioxide into nitrogen results in a much higher flow, which is similar to that induced by the evaporating ethanol droplet. Hence, the results presented in this section strongly indicate that buoyancy-driven flow is the origin of the flow observed around an evaporating droplet. The effects of molecular weight (solutal) and temperature (thermal) are both important in creating this flow. In this context, it can be seen from Fig. 3 that the direction of flow below the evaporating water droplet is downward. Although the solutal effect suggests that the flow should be upward, the thermal effect is dominant here. Owing to the low temperature of water during its evaporation, the surrounding gas (i.e., nitrogen) in the vicinity of the droplet probably also gets cooled and hence falls downwards.

The direction of the flow can be predicted from the expression for $\Delta\rho$ in Eq. (2). $\Delta\rho$, the difference between the surface and ambient densities, is negative (upward flow) if $M_v < M_g$ (for purely solutal convection) or $T_s > T_\infty$ (for purely thermal convection). However, for thermosolutal convection, the combined effect of temperature and molecular weight determines whether the gas in the vicinity of the droplet is lighter or heavier than the ambient gas. For water in nitrogen, although the molecular weight of water is less than that of nitrogen, the flow moves downward, which indicates that the thermal effect is dominant here. This can also be seen from the thermal and solutal Grashof numbers as listed in Table I. These can be obtained by considering only the solutal or thermal contributions in the expression for the density gradient in Eq. (2). Water vapour

TABLE II. Properties of water and ethanol,[25] thermal conductivity of steel,[26] and thermal conductivity of quartz[27] (used for the calculation of diffusion-driven evaporation rate and *Gr* values in Table I).

Configuration		T_s	Latent heat of vaporization	Vapour pressure	Thermal conductivity of suspender at 301 K
Suspender	Liquid	(K)	(kJ/kg)	(kPa)	(W/(m K))
Steel	Ethanol	288	937.14	4.30	14
Quartz	Ethanol	283	944.06	3.12	1.4
Steel	Water	293	2445.30	2.31	14
Quartz	Water	288	2451.10	1.91	1.4

being lighter than ambient nitrogen, the solutal Grashof numbers are negative. However, the thermal Grashof number which is positive dominates here. Hence, the net effect causes a downward flow.

There are of course other minor effects which can cause the flow in the droplet surroundings. One possibility is that the metallic needle containing the ethanol might cool the surrounding and hence cause the flow. However, the temperature of the needle was observed to be close to that of the ambient from the thermal images. The other possibility is of Marangoni convection inducing the flow in the surroundings. It has been reported earlier in the literature[2,4] that Marangoni convection is insignificant in the case of evaporating pendant water droplets. The presence of flow in the surroundings (with similar velocities as in the case of ethanol) even for evaporating water droplets in the present study indicates that the contribution of Marangoni convection to the flow is insignificant. Additionally, experiments were described earlier with the introduction of CO_2 gas into a nitrogen ambient at a flow rate similar to that of the ethanol vapour generation rate from an evaporating pendant ethanol drop. The molecular weights of ethanol and CO_2 are similar. The CO_2 introduced produced a flow very similar to that observed in the case of evaporating ethanol droplets. While Marangoni convection is expected to be present in the case of ethanol droplets, it is absent in the case of the gaseous CO_2 flow. Hence, the chances of Marangoni convection driving the surrounding flow for both water and ethanol drops are unlikely.

Table I also presents different experimental data and calculated diffusion-driven evaporation rates apart from Grashof numbers. The values of the physical properties used for these calculations are shown in Table II. The cases include a water droplet suspended from a metallic needle, a water droplet suspended from a quartz fibre, an ethanol droplet suspended from a metallic needle, and an ethanol droplet suspended from a quartz fibre. The thermal conductivities of the metallic needle and quartz are very different, as can be seen from Table II. The evaporation rate of ethanol from the metallic needle is highest among the four cases. The evaporation rate of ethanol from the quartz fibre is quite low and indeed closer to the evaporation rate of water from the metallic needle. The evaporation rate of water from the quartz fibre is the lowest.

By comparing the experimental and calculated evaporation rates, it can be observed that with the use of a quartz suspender, the evaporation rates (measured and diffusion driven) are closer, indicating that the suspender seems to play a more important role on the evaporation rate than the convective flow under the present conditions.

IV. CONCLUSIONS

We have directly observed flow around single droplets evaporating in nitrogen gas at atmospheric temperature and pressure. The magnitude of the velocity has been quantified by PIV measurements. The flow is seen to exist for both rapidly and slowly evaporating droplets (ethanol and water) with low Grashof numbers. The experiments conducted confirm that this flow originates from buoyant forces due to thermal and solutal effects. The flow is directed downward for both ethanol and water droplets evaporating in a nitrogen ambient, indicating the dominance of thermal buoyancy under these conditions.

[1] W. Niven, *The Scientific Papers of James Clerk Maxwell* (Dover Publications, Inc., New York, 1965).
[2] D. K. Mandal and S. Bakshi, "Internal circulation in a single droplet evaporating in a closed chamber," Int. J. Multiphase Flow **42**, 42–51 (2012).

[3] S. F. Chini and A. Amirfazli, "Understanding the evaporation of spherical drops in quiescent environment," Colloids Surf., A **432**, 82–88 (2013).

[4] J. J. Hegseth, N. Rashidnia, and A. Chai, "Natural convection in droplet evaporation," Phys. Rev. E **54**, 1640 (1996).

[5] R. Savino and S. Fico, "Transient Marangoni convection in hanging evaporating drops," Phys. Fluids **16**, 3738 (2004).

[6] G. Guèna, C. Poulard, M. Voué, J. De Coninck, and A. Cazabat, "Evaporation of sessile liquid droplets," Colloids Surf., A **291**, 191–196 (2006).

[7] R. N. O'Brien and P. Saville, "Investigation of liquid drop evaporation by laser interferometry," Langmuir **3**, 41–45 (1987).

[8] S. Dehaeck, A. Rednikov, and P. Colinet, "Vapor-based interferometric measurement of local evaporation rate and interfacial temperature of evaporating droplets," Langmuir **30**, 2002–2008 (2014).

[9] K. Sefiane, J. R. Moffat, O. K. Matar, and R. V. Craster, "Self-excited hydrothermal waves in evaporating sessile drops," Appl. Phys. Lett. **93**, 074103 (2008).

[10] K. Sefiane, A. Steinchen, and R. Moffat, "On hydrothermal waves observed during evaporation of sessile droplets," Colloids Surf., A **365**, 95–108 (2010).

[11] D. Brutin, B. Sobac, F. Rigollet, and C. Le Niliot, "Infrared visualization of thermal motion inside a sessile drop deposited onto a heated surface," Exp. Therm. Fluid Sci. **35**, 521–530 (2011).

[12] B. Sobac and D. Brutin, "Thermocapillary instabilities in an evaporating drop deposited onto a heated substrate," Phys. Fluids **24**, 032103 (2012).

[13] P. L. Kelly-Zion, C. J. Pursell, R. S. Booth, and A. N. VanTilburg, "Evaporation rates of pure hydrocarbon liquids under the influences of natural convection and diffusion," Int. J. Heat Mass Transfer **52**, 3305–3313 (2009).

[14] F. Carle, B. Sobac, and D. Brutin, "Experimental evidence of the atmospheric convective transport contribution to sessile droplet evaporation," Appl. Phys. Lett. **102**, 061603 (2013).

[15] G. J. Dunn, S. K. Wilson, B. R. Duffy, S. David, and K. Sefiane, "The strong influence of substrate conductivity on droplet evaporation," J. Fluid Mech. **623**, 329 (2009).

[16] A. M. Saada, S. Chikh, and L. Tadrist, "Numerical investigation of heat and mass transfer of an evaporating sessile drop on a horizontal surface," Phys. Fluids **22**, 112115 (2010).

[17] H. Gelderblom, A. G. Marín, H. Nair, A. V. Houselt, L. Lefferts, J. H. Snoeijer, and D. Lohse, "How water droplets evaporate on a superhydrophobic substrate," Phys. Rev. E **83**, 026306 (2011).

[18] Y. O. Popov, "Evaporative deposition patterns: Spatial dimensions of the deposit," Phys. Rev. E **71**, 036313 (2005).

[19] K. Sefiane, S. K. Wilson, S. David, G. J. Dunn, and B. R. Duffy, "On the effect of the atmosphere on the evaporation of sessile droplets of water," Phys. Fluids **21**, 062101 (2009).

[20] K. Gleason and S. A. Putnam, "Microdroplet evaporation with a forced pinned contact line," Langmuir **30**, 10548–10555 (2014).

[21] M. Jermy, "An economical droplet fog generator suitable for laser Doppler anemometry and particle imaging velocity seeding," Exp. Fluids **33**, 321–322 (2002).

[22] W. Thielicke and E. J. Stamhuis, PIVlab-Time-Resolved Digital Particle Image Velocimetry Tool for MATLAB, 2014, http://dx.doi.org/10.6084/m9.figshare.1092508.

[23] W. Thielicke, "The flapping flight of birds-analysis and application," Ph.D. thesis, Rijksuniversiteit Groningen, 2014.

[24] See supplementary material at http://dx.doi.org/10.1063/1.4935355 for supplemental videos: Movie 1 shows the flow below a pendant ethanol droplet, while Movie 2 shows the flow below an evaporating water droplet. Images were taken at 50 frames/s in both cases and are played back at 5 frames/s.

[25] P. Linstrom and W. Mallard, *NIST Chemistry WebBook*, NIST Standard Reference Database No. 69, National Institute of Standards and Technology, Gaithersburg, MD, 2014.

[26] R. S. Graves, T. G. Kollie, D. L. McElroy, and K. E. Gilchrist, "The thermal conductivity of AISI $_{304}$L stainless steel," Int. J. Thermophys. **12**, 409–415 (1991).

[27] A. Sugawara, "Precise determination of thermal conductivity of high purity fused quartz from 0 to 650 °C," Physica **41**, 515–520 (1969).